A MACHINE LEARNING APPROACH TO QUANTIFY DISSOLUTION KINETICS OF POROUS MEDIA

Huaxinyu Wang,[1] Chenghai Li,[2] Wei-W. Xing,[3] Yanan Ye,[4] & Peng Wang[3,5,*]

[1]*Department of Energy Resources Engineering, Stanford University, 367 Panama Street, Stanford, CA 94305, USA*

[2]*School of Mathematical Sciences, Beihang University, Beijing, China*

[3]*School of Integrated Circuit Science and Engineering, Beihang University, Beijing, China*

[4]*School of Mathematical Sciences, Peking University, Beijing, China*

[5]*LMIB & Beijing Advanced Innovation Center for Big Data and Brain Computing, Beijing, China*

*Address all correspondence to: Peng Wang, School of Integrated Circuit Science and Engineering, Beihang University, Beijing, China, E-mail: wang.peng@buaa.edu.cn

Original Manuscript Submitted: 3/29/2021; Final Draft Received: 6/2/2021

Microspheres are popular drug products comprises of drug particles embedded in a matrix of wax and pore former. Microstructural attributes of these beads affect the overall dissolution release kinetics of the product. Due to the complex geometry and high computational cost associated with pore-scale simulations, the impact of microstructural attributes on the drug release rate is yet to be well studied. In this paper, we propose a machine learning framework to examine the drug release rate by estimating the temporal profile of the effective diffusion coefficient of the dissolved drug through the pores. By incorporating a statistical description of the pore structure via the Minkowski functionals, our model can also provide probabilistic distribution of the effective property at a given time. Leveraging such efficient numerical framework, we conduct sensitivity analysis and rank the geometric parameters according to their impacts on the drug release rate.

KEY WORDS: *porous media, Minkowski functionals, Gaussian process, drug dissolution kinetics*

1. INTRODUCTION

Porous media is ubiquitous and has wide applications in natural and engineering systems. From oil extraction to electrodes made of nanocarbon tubes, geometric structure at the pore scale exerts significant impact on macroscopic properties such as permeability, effective diffusion coefficients, and many others.

In past decades, the porous microsphere has become an increasingly popular form of drug product in the pharmaceutical industry. By regulating the release rate of drug particles into the human body, such products not only help improve drug delivery efficiency by maintaining a relatively constant level of concentration, but also help reduce potentially lethal damage from overdoses. However, stochastic manufacture processes and variations render the geometric structures of those microspheres random. Meanwhile, high-fidelity simulation at the pore scale often incurs high computational cost, and a thorough analysis of every microsphere in a normal dose, which amounts to the hundreds in a capsule, is thus unrealistic.

To address similar modeling and simulation problems that have occurred in other applications of porous media, a proliferation of numerical frameworks has been developed over the years. The multilevel Monte Carlo (MLMC) method (Efendiev et al., 2013; Icardi et al., 2016) and the variance reduction techniques (Blanc et al., 2015) are classical approaches to random porous media. They are easy to implement, and the overall computational cost may be reduced by preconditioning high-fidelity (fine-scale) results with the low-fidelity (coarse-scale) ones. Alternatively, Wang et al. (2018) proposed an uncertainty quantification approach by constructing the polynomial chaos expansion of the target macroscopic property using Minkowski functionals as geometric parameters. Although it was shown to have superior numerical efficiency to classic Monte Carlo simulations (MCS) in capturing the statistical distribution of the macroscopic permeability, its theoretical dependance on the functional smoothness between model inputs and outputs may become problematic in practical applications. With the recent rise of machine learning, researchers have also developed neural networks (Wu et al., 2019, 2018) to directly link pore structures to effective properties. However, owing to the higher computational cost of processing complex images, current works based on neural networks remain focused on two-dimensional cases.

In this paper, we propose a novel and efficient numerical framework, based on the machine learning technique, to estimate the macroscopic diffusion coefficients of three-dimensional porous microspheres. To be specific, Minkowski functionals are employed as inputs to our Gaussian Process, while the temporal profile of effective diffusion coefficients are the outputs. By building such a model, one can also incorporate random variations of the pore structures and thus obtain full statistical information, such as the probabilistic density function, of the macroscopic property without incurring such high computational costs as MCS.

The subsequent contents of this paper are organized as follows: in Section 2 we formulate the general problems in determining the effective diffusion coefficients of a three-dimensional microsphere. Section 3 provides details of our numerical framework in tackling such problems. Its evaluation via a large number of porous samples is then conducted and discussed in Section 4. Finally, the overall conclusion is summarized in Section 5.

2. PROBLEM FORMULATION

Unless specificed otherwise, vectors $\mathbf{u}$ will be represented by lowercase boldface letters, while uppercase boldface letters will be reserved for matrices $\mathbf{U}$. The superscripts in $\mathbf{U}^{\mathrm{T}}$ and $\mathbf{U}^{-1}$ are the matrix transpose, and the inverse of $\mathbf{U}$, respectively.

Microspheres are engineered composites that are comprised of drug (active pharmaceutical ingredient, API) particles embedded in a matrix of insoluble wax and soluble pore former. As shown via the microscan in Fig. 1, the drug particle is of elliptical shape. Once it has contacted fluids in the human body, the pore former dissolves away and then undergoes solidification and

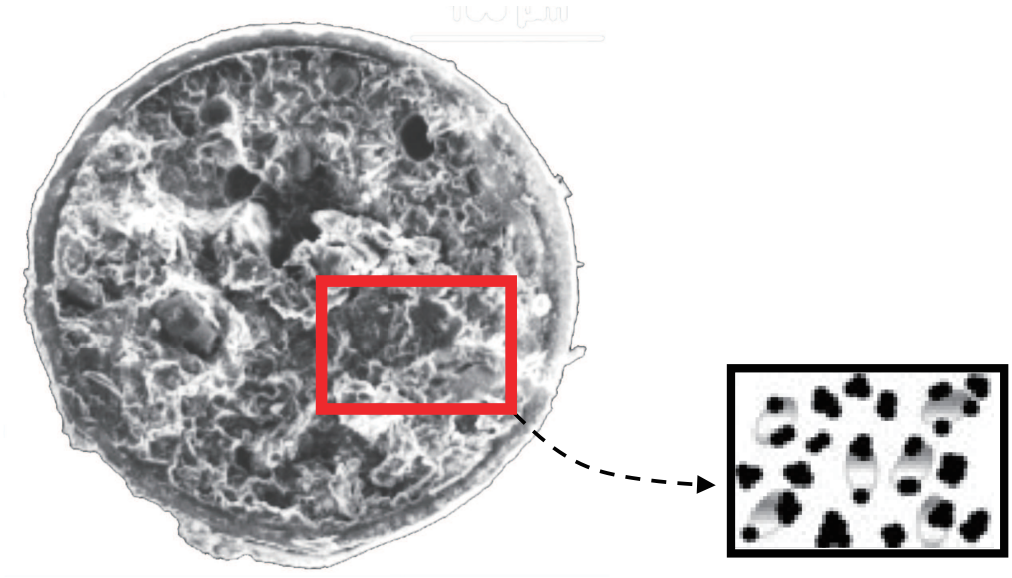

FIG. 1: A microscan of the cross section of a microsphere based on Bartlett (2017) and its schematics of drug particles (elliptical shapes), insoluble wax (dark dots), and the pore (white space)

phase separation. It leaves behind a porous network of channels in the microspheres, which allows the API to release.

In the absence of a velocity field, the API particles migrate within the porous media by molecular diffusion (Beck and Schultz, 1970). At the pore scale, such hindered movement of molecules of a substance among molecules of the solute, for example, water, can be described by a modified Fick's law:

$$\frac{\partial c}{\partial t} = D\nabla^2 c, \tag{1}$$

where c is the concentration of drug particles and D is its intrinsic diffusion coefficient. We introduce flux J_{m}, defined as the number of API particles flowing through a surface area per unit time:

$$\mathrm{d}J_{\mathrm{m}} = \frac{\partial c}{\partial t}\mathrm{d}S = D\nabla c. \tag{2}$$

Structural attributes of the microsphere, such as compositions of the API, wax and pore former, pore sizes, spatial distribution of API and pores, etc., affect the dissolution of the API at pore scale in each passage. Collectively, one may describe the macroscopic release kinetics with an effective diffusion coefficient by integrating Eq. (1) over the entire boundary surface:

$$J_{\mathrm{m}} = \int_A \frac{\partial c}{\partial t}\mathrm{d}S = -D_{\mathrm{eff}}\nabla c. \tag{3}$$

In practice, pores in the microsphere range from 10–1000 nanometers, the average size of API particle is 10–40 micrometers, and the microsphere is about 250 micrometers in size. Hence

a thorough pore-scale simulation of the hindered diffusion process over the entire domain is expensive. Meanwhile, manufacturing conditions may affect the degree of separation after the pore former dissolves and thus the nature of heterogeneity of the porous network. It no doubt adds complexity to the modeling of effective diffusion coefficients. In subsequent study, our goal is to construct an efficient numerical scheme in order to study the impact of drug product micro-structural attributes on the macroscopic drug release rate.

3. METHODOLOGY

In this section, we outline our numerical methodology to construct a machine learning approach in order to capture the temporal evolution of the effective diffusion coefficient of a microsphere. Given the porous structure, the main feature of our method is its adoption of the Minkowski functionals to characterize the domain geometry and thus its numerical efficiency in constructing a model with relatively fewer samples from pore-scale simulations. To be specific, our framework consists of the following steps:

1. Generate representative samples of microspheres with drug particles, insoluble wax, and pores.

2. Obtain the statistics of Minkowski functionals of those samples.

3. Perform pore-scale simulations on hindered diffusion through narrow pores and then calculate the corresponding effective diffusion coefficient.

4. Construct the surrogate model of effective diffusion coefficients using the machine learning approach, such as Gaussian Process, with a subset of solutions from step 3.

We now present details of the framework.

3.1 Pore Samples Generation

In practice, a microscan of the microsphere is expensive. To complement the shortage of those experimental scans, we propose a numerical method to generate representative samples. Our algorithm consists of two modules: one that randomly scatters the drug particles in a fixed volume according to a preset drug volume ratio V_{API}; the other is the quartet structure generation set (QSGS) method (Wang and Pan, 2009) which generates random porous media of wax and pore former. Finally, we choose the inscribed sphere in this cube to represent the actual porous microsphere. In all, there are four parameters to be set: the drug volume ratio V_{API}, the wax volume ratio V_{wax}, the given probability p_{wax} to randomly place the wax core, and the growth probability p^i_{vw} of pore at direct e_i.

We note here that the QSGS method is selected for its easy implementation and close resemblance to the actual forming progress of pores (Wang et al., 2007). Without loss of generality, it can be replaced with other numerical methods to generate porous media. For example, one may employ a convolution varietal auto-encoder (CVAE) (Cang et al., 2018) or generative adverse network (GAN) (Feng et al., 2019; Mosser et al., 2017) using sufficient microscan images. To sum up, our algorithm can be written as follows:

Algorithm 1: Constraint multiphase porous sample generation using modified QSGS

1. Drug particles generation:
while *Total drug volume ratio* $<$ *than the preset drug volume ratio* V_{API} **do**
  Randomly select:
  the potential center of drug from all available positions;
  the rotation angle of elliptical shape;
  if *the ellipse domain has not been occupied* **then**
    an elliptical drug particle will be generated here;
  end
end
2. Porous media generation:
Randomly distribute the potential wax core in the rest of domain excluded from drug, for a given probability p_{wax};
while *Total wax volume ratio* $<$ *Preset wax volume ratio* V_{wax} **do**
  Store the wax position;
  for *each direction* e_i **do**
    for *each wax voxel (denote its coordinate as* z*)* **do**
      if $z + e_i$ *is not wax, drug, or out of boundary* **then**
        change the voxel to wax using probability p^i_{vw};
      end
    end
  end
end
3. Randomly delete the excessive wax volume to ensure that the total wax volume ratio exactly matches the preset ratio.

3.2 Minkowski Functionals

The effective diffusion coefficient is strongly affected by the morphological characteristics of the void–solid interface of porous samples (Scholz et al., 2015). In our numerical framework, we employ the Minkowski functionals (Mecke, 2000; Mecke and Stoyan, 2000, 2008) to characterize the geometric features of a porous structure. They can be extracted from the binary image of a given sample, such as its microscan, and are normalized by the volume of the image (Vogel et al., 2010).

A three-dimensional porous media such as our microsphere can be measured by four Minkowski functionals $\boldsymbol{m} = [m_1, m_2, m_3, m_4]$:

- Porosity m_1: the ratio of the void volume V_0 to the total volume V_{tot}:

$$m_1 = \frac{V_0}{V_{\mathrm{tot}}}. \tag{4a}$$

- Surface area m_2: a measure relevant to the interaction of solutes at the pore–solid interface and thus affects the dissolution process:

$$m_2 = \frac{1}{V_{\mathrm{tot}}} \int_{\delta X} \mathrm{d}S, \tag{4b}$$

  where δX and $\mathrm{d}S$ denotes the void surface and the surface element, respectively.

- Mean principal curvature m_3: a description of the pore shape, which affects the energy density of wetting fluid (Wang et al., 2018):

$$m_3 = \frac{1}{2V_{\text{tot}}} \int_{\delta X} \left(\frac{1}{r_1} + \frac{1}{r_2} \right) \mathrm{d}S. \tag{4c}$$

  Here r_1 and r_2 denote the principle curvature of the surface element.

- Euler characteristic m_4: a measure on the connectivity of the porous medium:

$$m_4 = \frac{1}{4\pi V_{\text{tot}}} \int_{\delta X} \frac{\mathrm{d}S}{r_1\, r_2}. \tag{4d}$$

It is noted here that the Minkowski functionals provide statistical descriptions on the whole porous structure. In other words, despite that the two structures generated with identical $\boldsymbol{m}$ may exhibit microscopic differences at the pore scale, their macroscopic properties remain identical (Berchtold, 2007). In our study, we employ the Ohser–Mücklich estimator (Berchtold, 2007) to compute the Minkowski functionals. A detailed yet easy derivation can be found in the appendix of an earlier study (Wang et al., 2018), and the numerical codes can be downloaded upon request.

3.3 Pore-Scale Simulation of Hindered Diffusion

Various numerical methods can be applied to simulate the hindered diffusion process in a porous media. For easy implementation, the lattice Boltzmann (LBM) method (Chen and Doolen, 1998; Girimaji, 2013; Meng and Guo, 2015) is adopted here and we select the lattice Bhatnagar–Gross–Krook (lattice BGK) scheme (Bhatnagar et al., 1954), whose evolution equation can be written as follows:

$$f_i(\mathbf{x} + \mathbf{u}_i \Delta t,\, t + \Delta t) - f_i(\mathbf{x}, t) = -\omega [f_i(\mathbf{x}, t) - f_i^{\text{eq}}(\mathbf{x}, t)], \tag{5a}$$

where i is the discrete velocity index, and $f_i(\mathbf{x}, t)$ denotes the particle distribution at the physical point $(\mathbf{x}, t)$ and at the velocity $\mathbf{u}_i$. The discrete time step and lattice unit are represented by Δt and Δx, respectively. We employ the Chapman–Enskog expansion (Girimaji, 2013) for the relaxation frequency ω:

$$\omega = \frac{2\Delta x^2}{2d\Delta t\, D + \Delta x^2}, \tag{5b}$$

in which $d = 3$ is space dimension.

Since there is no advection in the hindered diffusion process, the equilibrium distribution function f_i^{eq} in Eq. (5a) becomes

$$f_i^{\text{eq}}(\mathbf{x}, t) = w_i \sum_{i=1}^{n} f_i(\mathbf{x}, t), \tag{6}$$

where n is the maximum discrete velocity index, and w_i is the weight factor of the velocity $\mathbf{u}_i$.

To discretize the velocity space, one can employ the three-dimension 19-velocity (D3Q19) model below:

$$\mathbf{u}_i = \begin{cases} u_{\rm ls}(0,0,0) & i = 0 \\ u_{\rm ls}(\pm 1,0,0),\ u_{\rm ls}(0,\pm 1,0),\ u_{\rm ls}(0,0,\pm 1) & i = 1,\ldots,6 \\ u_{\rm ls}(\pm 1,\pm 1,0),\ u_{\rm ls}(\pm 1,0,\pm 1),\ u_{\rm ls}(0,\pm 1,\pm 1) & i = 7,\ldots,18 \end{cases}, \tag{7}$$

with $u_{\rm ls} = \Delta x/\Delta t$ is lattice speed.

For simplification, we assume the solid drug particle instantaneously dissolves into the surrounding bulk solution at its original location. Zero concentration is prescribed at the outer surface of the drug particle, while a "bounce-back" boundary condition is assumed at the surface of the wax voxels. By fixing a total simulation time step $N_{\rm t}$, our lattice BGK algorithm can be summed up as the following:

Algorithm 2: LBGK-D3Q19

Initialization:

- $c(\mathbf{x},0) = 1$ for drug voxel and $c(\mathbf{x},0) = 0$ otherwise
- Calculate the particle distribution function at all velocities: $i = 1,\ldots,19$

$$f_i(\mathbf{x},0) = f_i^{\rm eq}(\mathbf{x},0) = w_i\, c(\mathbf{x},0).$$

for $t = 0;\ \ t < N_{\rm t};\ \ t++$ **do**

Calculate and store the sum of $c(\mathbf{x},t)$ for all spatial points $\mathbf{x}$.

$$\begin{aligned} f_i(\mathbf{x}+\mathbf{u}_i\Delta t, t) &= f_i(\mathbf{x},t), \\ f_i(\mathbf{x},t+1) &= f_i(\mathbf{x},t) + \omega[f_i^{\rm eq}(\mathbf{x},t) - f_i(\mathbf{x},t)]. \end{aligned}$$

end

3.4 Gaussian Process Surrogate Modeling

Although one may employ the generalized polynomial chaos expansion (gPC) to construct the surrogate model of macroscopic parameters using data from pore-scale simulations (Wang et al., 2018), functional relations between the inputs variables, such as the Minkowski functionals $\mathbf{m}$ Eq. (4), and the effective parameters are not necessarily smooth. In such case, the gPC model would require a higher order to converge and thus would incur high computational cost, i.e., more high-fidelity data. In this work, we propose to construct the surrogate model using machine learning methods: in particular, the Gaussian process (GP) (Kennedy et al., 2006; Kennedy and O'Hagan, 2001; Rasmussen and Williams, 2006; Santner et al., 2003).

Since the output of the neural network, the effective diffusion coefficient $D_{\rm eff}(t,\mathbf{m})$, varies with time as drugs release out of the porous media, we treat it as a function rather than a single variable. In other words, $D_{\rm eff}(t,\mathbf{m})$ is fully discretized in time at the pore-scale simulation time steps, and the GP output $\mathbf{y}(\mathbf{m}) \in \mathbb{R}^{N_{\rm t}}$ is represented by a finite vector:

$$\mathbf{y}(\mathbf{m}) = [D_{\rm eff}(t_1,\mathbf{m}),\ldots,D_{\rm eff}(t_{N_{\rm t}},\mathbf{m})]^{\rm T}. \tag{8}$$

To solve this multivariate GP problem (Conti and O'Hagan, 2010; Xing et al., 2020, 2015, 2016), we select the class separable Gaussian process (Conti and O'Hagan, 2010) with respect to the correlation between the inputs and the outputs. Here the functional prior for output vector $\mathbf{y}(\mathbf{m})$ is specified with a zero mean function:

$$\mathbf{y}(\mathbf{m}) \sim \mathcal{N}(0, k(\mathbf{m}_i, \mathbf{m}_j)\mathbf{\Sigma}), \qquad i, j = 1, \ldots, N_{\mathrm{d}}, \tag{9}$$

and $k(\mathbf{m}_i, \mathbf{m}_j)$ represents a kernel function for the corresponding inputs from a number of N_{d} data: $\mathbf{\Sigma}$ is the correlation between output variables. We note here that it is a nontrivial task to choose the right kernel function for any specific application. In the absence of prior knowledge, one can select the automatic relevance determinant (ARD) kernel (Rasmussen and Williams, 2006):

$$k(\mathbf{m}_i, \mathbf{m}_j) = \theta_0 \exp\big[-(\mathbf{m}_i - \mathbf{m}_j)\ \mathrm{diag}(\theta_1, \ldots, \theta_l)(\mathbf{m}_i - \mathbf{m}_j)^{\mathrm{T}}\big], \tag{10}$$

where $(\theta_0, \ldots, \theta_l)$ are the hyperparameters of our neural network. The ARD formulation automatically scales the weight of each input variable that contributes to the outputs.

The functional prior for outputs Eq. (9) indicates that, given any finite number N_{d} of data, e.g., inputs data $\mathbf{M} = [\mathbf{m}_1, \ldots, \mathbf{m}_{N_{\mathrm{d}}}]^{\mathrm{T}}$ plus the corresponding outputs $\mathbf{Y} = [y(\mathbf{m}_1), \ldots, y(\mathbf{m}_{N_{\mathrm{d}}})]^{\mathrm{T}}$, the joint distribution becomes a matrix Gaussian,

$$\mathbf{Y} \sim \mathcal{MN}(0, \mathbf{K}, \mathbf{\Sigma}). \tag{11}$$

Note that the covariance matrix between the model inputs is denoted as $[\mathbf{K}]_{ij} = k(\mathbf{m}_i, \mathbf{m}_j)$.

Now the neural network consists of hyperparameters $(\theta_0, \ldots, \theta_l, \mathbf{\Sigma})$, which can be optimized by maximizing the likelihood of the matrix Eq. (11):

$$\mathcal{L} = \frac{1}{2} \ln |\mathbf{\Sigma} \otimes \mathbf{K}| - \frac{1}{2} \mathrm{vec}(\mathbf{Y})^{\mathrm{T}} (\mathbf{\Sigma} \otimes \mathbf{K})^{-1} \mathrm{vec}(\mathbf{Y}) - \frac{N_{\mathrm{d}}\, t_{N_{\mathrm{t}}}}{2} \ln(2\pi). \tag{12}$$

The major cost of our neural network stems from the inversion of $\mathbf{\Sigma} \otimes \mathbf{K}$. Using the Kronecker product trick (Zhe et al., 2019), one can reduce such cost to $\mathcal{O}(N^3 + T^3)$ and $\mathcal{O}(N^2 + T^2)$ for time and space complexity, respectively. Meanwhile, the computation cost can be further reduced by setting $\mathbf{\Sigma}$ to an identical matrix, $\mathbf{\Sigma} = \mathbf{I}$, with no compromise on the predictive accuracy (Alvarez et al., 2012; Xing et al., 2020).

Finally, for a new input $\mathbf{m}_*$, different from the existing (training) data, one can apply the conditioning rules of a joint Gaussian distributions (Rasmussen and Williams, 2006) and compute the posterior distribution p of outputs, its means $\boldsymbol{\mu}$ and variances $\mathbf{v}$ as

$$p(\mathbf{y}(\mathbf{m}_*) \mid \mathbf{M}, \mathbf{Y}) = \mathcal{N}(\mathbf{y}(\mathbf{m}_*) \mid \mu(\mathbf{m}_*), \mathbf{v}(\mathbf{m}_*)), \tag{13a}$$

$$\boldsymbol{\mu}(\mathbf{m}_*) = \mathbf{k}(\mathbf{m}_*)^{\mathrm{T}}\, \mathbf{K}^{-1}\, \mathbf{Y}, \tag{13b}$$

$$\mathbf{v}(\mathbf{m}_*) = \big(k(\mathbf{m}_*, \mathbf{m}_*) - \mathbf{k}(\mathbf{m}_*)^{\mathrm{T}}\, \mathbf{K}^{-1}\, \mathbf{k}(\mathbf{m}_*)\big)\mathbf{I}, \tag{13c}$$

where $\mathbf{k}(\mathbf{m}_*) = [k(\mathbf{m}_*, \mathbf{m}_1), \ldots, k(\mathbf{m}_*, \mathbf{m}_{N_{\mathrm{d}}})]^{\mathrm{T}}$ is the vector of covariances between the new inputs $\mathbf{m}_*$ and the existing (training) data of inputs $\mathbf{M}$.

4. RESULTS AND DISCUSSION

In this section, we evaluate our numerical framework via a set of randomly generated 3D porous microspheres. A sensitivity analysis is also conducted to examine the impacts on effective diffusion coefficient from the four Minkowski functionals. Unless specified otherwise, all quantities

are dimensionless. For the porous samples, a total of 2000 cubes of pixel size $128 \times 128 \times 128$ are generated using the modified QSGS Algorithm 1. Pill samples are cut from those cubes as an inscribed microsphere of with a radius of 64 pixels. In the algorithm, we set the API volume ratio as $V_{\mathrm{API}} = 0.05$ and the wax volume ratio as a uniform random variable, $V_{\mathrm{wax}} \sim \mathcal{U}(0.45, 0.75)$. The given probability to locate the wax core is taken as $p_{\mathrm{wax}} = 0.01$, and the growth probability p^i_{vw} is taken as

$$p^i_{\mathrm{vw}} = \begin{cases} 0.20, & \text{if the direction } e_i \text{ is in parallel to the axis of Cartesian coordinates;} \\ 0.05, & \text{otherwise} \end{cases} \tag{14}$$

to ensure a balance of pore growth in all directions. As shown in Fig. 2 with the cross section of the sphere sample, the lighter shaded or blue parts represent insoluble wax, while darker shaded or red is a realization of randomly scattered drug particles. The rest of the domain is pore former, which swiftly dissolves to channel after contacting the solute.

Figure 3 shows the histograms of all four Minkowski functionals computed from the 2000 samples. Since porosity, the first Minkowski functional m_1, is directly related to the setting parameters V_{API} and V_{wax} in generating the samples, its probability distribution is similar to that of the wax volume ratio, i.e., a uniform distribution. For the pore-scale simulations, we set a total time steps of 50,000 to reach a steady state of the effective diffusion coefficient. Two hundred samples, a fraction of the total 2000 sets, are utilized to train our neural network. Figure 4 presents the outputs of the effective diffusion coefficient at all time steps, computed

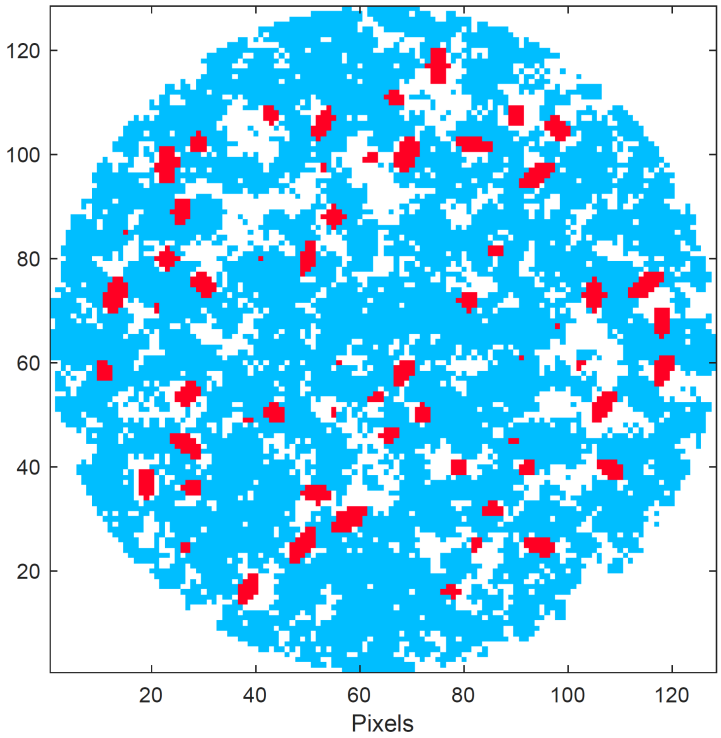

FIG. 2: The cross-sectional image of a microsphere sample generated from the modified QSGS algorithm

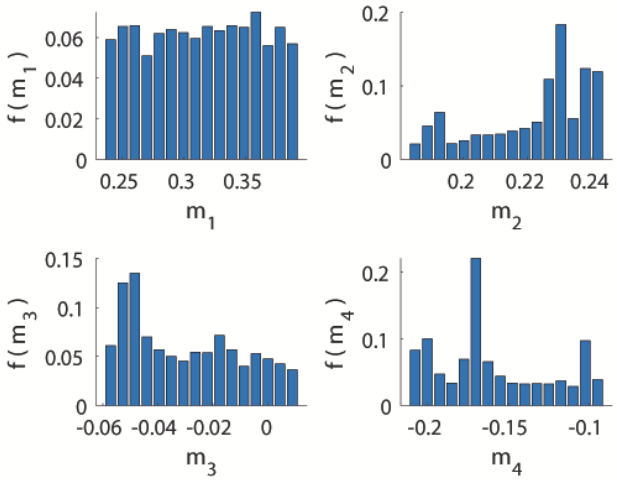

FIG. 3: Histograms of the four Minkowski functionals out of 2000 samples

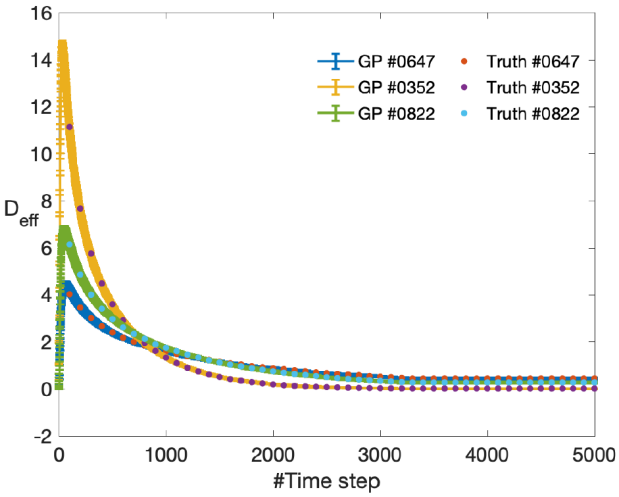

FIG. 4: D_{eff} comparsion between LBM result and GP prediction

from the GP and the lattice BGK method, respectively, using three randomly selected porous microspheres outside the training data. It is clear that our machine learning model provides a good prediction on the evolution of D_{eff} for a given porous structure.

For a more comprehensive analysis, we plot the time profiles of the mean and standard deviations of the effective diffusion coefficient of all 2000 samples, computed from our neural network in Fig. 5. Results from the same 2000 samples using Monte Carlo simulations are also included for comparison. As expected, there is a good match between the exhaustive MCS and the GP outputs. For a closer look, Fig. 6 presents the probabilistic density function (PDF) of the effective diffusion coefficient $f_{D_{\text{eff}}}$ using our framework and MCS, respectively, at four time

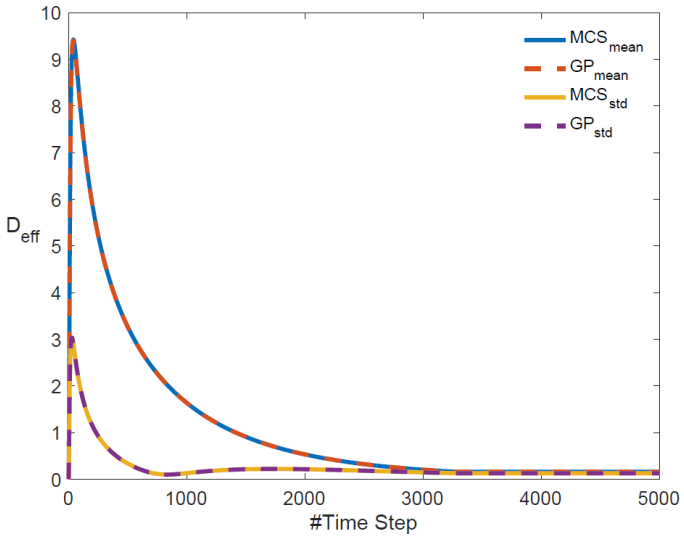

FIG. 5: Temporal profiles of mean and standard deviation of D_{eff}, computed from GP and MCS, respectively

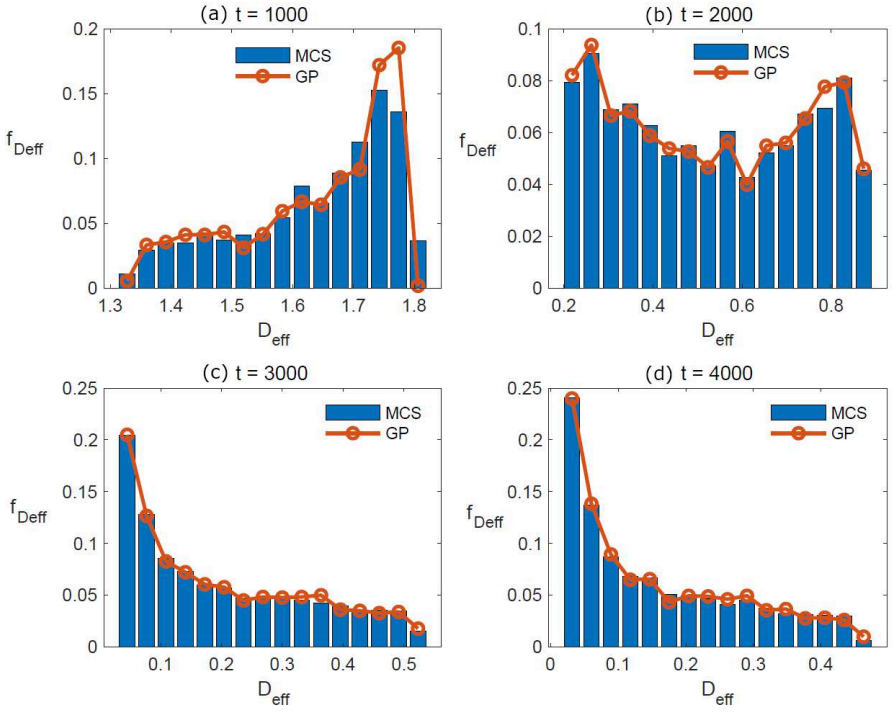

FIG. 6: PDF of D_{eff} computed from GP and MCS, respectively, at four time steps: a) 1000, b) 2000, c) 3000, and d) 4000

steps: a) 1000, b) 2000, c) 3000, and d) 4000. One can see the center of the PDF gradually shifts from right to left as time elapses and remains relatively steady at latter time. This is also expected from Fig. 5 since the dissolution process eventually reaches a steady state of relatively constant release. In general, the neural network well captures not only the bulk of the statistical distribution of the macroscopic property but also its tails. All the results above demonstrate the effectiveness of our machine learning framework in predicting the effective diffusion coefficients while using only 10 percent of the high-fidelity samples as that of MCS.

To examine the impacts of porous structure on the effective property, a sensitivity analysis was conducted. Table 1 shows the kernel parameters corresponding to each Minkowski functional in GP training.

We note that the Minkowski functional with a smaller kernel parameter indicates stronger influence on the overall predictive model. Henceforth, porosity, m_1, with kernel value of 4.245 is the dominant parameter among all four geometric parameters, whereas pore connectivity, m_4, casts the smallest impacts on the effective diffusion coefficient. For m_2 and m_3, surface area is less important in drug release kinetics than the mean principal curvature.

5. CONCLUSION

We propose a numerical framework based on machine learning to describe the drug release kinetics of a porous microsphere consisting of drug particles, soluble wax, and insoluble pore former. In our framework, geometry of the microsphere is characterized with the Minkowski functionals and serves as inputs to the neural network. Our work leads to the following conclusions:

- Using the Gaussian process, our neural network provides accurate estimation of the temporal profiles of effective diffusion coefficients for a given porous microsphere.
- By incorporating random structure at the pore scale, the proposed model can also compute full statistical distributions of the effective diffusion coefficient at a given time.
- Compared to Monte Carlo simulations, the proposed model requires far less data to quantify the predictive uncertainty of the effective property due to random geometry.
- Our sensitivity analysis found that porosity is the dominant geometry parameter on the overall drug dissolution kinetics.

ACKNOWLEDGMENTS

This research was partially funded by the National Key Research and Development Program of China (Grant No. 2017YFB0701700 and Grant No. 2018YFB0703902). H. Wang was also supported by the Computational Mathematics program of AFOSR (Grant No. FA9550-07-1-0139).

TABLE 1: Gaussian process kernel parameters of each Minkowski functionals

Minkowski functional	m_1	m_2	m_3	m_4
Kernel parameter	4.2451	3.2605e+03	50.6913	1.2591e+05

REFERENCES

Alvarez, M.A., Rosasco, L., and Lawrence, N.D., Kernels for Vector-Valued Functions: A Review, *Found. Trends® Mach. Learn.*, vol. **4**, no. 3, pp. 195–266, 2012.

Bartlett, J.A., Oral Multiparticulates as a Pediatric Platform: How to Make Good Medicines Not Taste Bad, *AAPS Annual Meeting*, Pfizer Inc., 2017.

Beck, R.E. and Schultz, J.S., Hindered Diffusion in Microporous Membranes with Known Pore Geometry, *Science*, vol. **170**, no. 3964, pp. 1302–1305, 1970.

Berchtold, M.A., Modelling of Random Porous Media Using Minkowski-Functionals, PhD, ETH Zurich, 2007.

Bhatnagar, P.L., Gross, E.P., and Krook, M., A Model for Collision Processes in Gases. I. Small Amplitude Processes in Charged and Neutral One-Component Systems, *Phys. Rev.*, vol. **94**, pp. 511–525, 1954.

Blanc, X., Bris, C., and Legoll, F., Some Variance Reduction Methods for Numerical Stochastic Homogenization, 2015. arXiv: 150902389

Cang, R., Li, H., Yao, H., Jiao, Y., and Ren, Y., Improving Direct Physical Properties Prediction of Heterogeneous Materials from Imaging Data via Convolutional Neural Network and a Morphology-Aware Generative Model, *Comput. Mater. Sci.*, vol. **150**, pp. 212–221, 2018.

Chen, S. and Doolen, G.D., Lattice Boltzmann Method for Fluid Flows, *Ann. Rev. Fluid Mech.*, vol. **30**, no. 1, pp. 329–364, 1998. DOI: 10.1146/annurev.fluid.30.1.329

Conti, S. and O'Hagan, A., Bayesian Emulation of Complex Multi-Output and Dynamic Computer Models, *J. Statist. Plann. Inference*, vol. **140**, pp. 640–651, 2010.

Efendiev, Y., Kronsbein, C., and Legoll, F., Multi-Level Monte Carlo Approaches for Numerical Homogenization, 2013. arXiv: 13012798

Feng, J., He, X., Teng, Q., Ren, C., Chen, H., and Li, Y., Reconstruction of Porous Media from Extremely Limited Information Using Conditional Generative Adversarial Networks, *Phys. Rev. E*, vol. **100**, no. 3, p. 033308, 2019.

Girimaji, S., Lattice Boltzmann Method: Fundamentals and Engineering Applications with Computer Codes, *AIAA J.*, vol. **51**, no. 1, pp. 278–279, 2013. DOI: 10.2514/1.J051744

Icardi, M., Boccardob, G., and Tempone, R., On the Predictivity of Pore-Scale Simulations: Estimating Uncertainties with Multilevel Monte Carlo, *Adv. Water Resour.*, vol. **95**, pp. 46–60, 2016.

Kennedy, M., Anderson, C., Conti, C., and O'Hagan, A., Case Studies in Gaussian Process Modelling of Computer Codes, *Reliab. Eng. Syst. Safety*, vol. **91**, pp. 1301–1309, 2006.

Kennedy, M.C. and O'Hagan, A., Bayesian Calibration of Computer Models, *J. R. Stat. Soc. Ser. B (Stat. Methodol.)*, vol. **63**, no. 3, pp. 425–464, 2001.

Mecke, K.R., Additivity, Convexity, and Beyond: Applications of Minkowski Functionals in Statistical Physics, *Statistical Physics and Spatial Statistics*, K.R. Mecke and D. Stoyan, Eds., Berlin-Heidelberg: Springer, pp. 111–184, 2000.

Mecke, K.R. and Stoyan, D., *Statistical Physics and Spatial Statistics: The Art of Analyzing and Modeling Spatial Structures and Pattern Formation*, Vol. 554, Berlin: Springer Science and Business Media, 2000.

Mecke, K.R. and Stoyan, D., *Morphology of Condensed Matter: Physics and Geometry of Spatially Complex Systems*, Vol. 600, Berlin: Springer, 2008.

Meng, X. and Guo, Z., Multiple-Relaxation-Time Lattice Boltzmann Model for Incompressible Miscible Flow with Large Viscosity Ratio and High Péclet Number, *Phys. Rev. E*, vol. **92**, p. 043305, 2015. DOI: 10.1103/PhysRevE.92.043305

Mosser, L., Dubrule, O., and Blunt, M.J., Reconstruction of Three-Dimensional Porous Media Using Generative Adversarial Neural Networks, *Phys. Rev. E*, vol. **96**, no. 4, p. 043309, 2017.

Rasmussen, C.E. and Williams, C.K.I., *Gaussian Processes for Machine Learning*, Cambridge, MA: MIT Press, 2006.

Santner, T., Williams, B., and Notz, W., *The Design and Analysis of Computer Experiments*, Berlin: Springer, 2003.

Scholz, C., Wirner, F., Klatt, M.A., Hirneise, D., Schröder-Turk, G.E., Mecke, K., and Bechinger, C., Direct Relations between Morphology and Transport in Boolean Models, *Phys. Rev. E*, vol. **92**, p. 043023, 2015. DOI: 10.1103/PhysRevE.92.043023

Vogel, H.J., Weller, U., and Schlüter, S., Quantification of Soil Structure Based on Minkowski Functions, *Comput. Geosci.*, vol. **36**, no. 10, pp. 1236–1245, 2010.

Wang, M. and Pan, N., Elastic Property of Multiphase Composites with Random Microstructures, *J. Comput. Phys.*, vol. **228**, no. 16, pp. 5978–5988, 2009.

Wang, M., Wang, J., Pan, N., and Chen, S., Mesoscopic Predictions of the Effective Thermal Conductivity for Microscale Random Porous Media, *Phys. Rev. E*, vol. **75**, p. 036702, 2007. DOI: 10.1103/PhysRevE.75.036702

Wang, P., Chen, H., Meng, X., Jiang, X., Xiu, D., and Yang, X., Uncertainty Quantification on the Macroscopic Properties of Heterogeneous Porous Media, *Phys. Rev. E*, vol. **98**, no. 3, 2018. DOI: 10.1103/PhysRevE.98.033306

Wu, H., Fang, W.Z., Kang, Q., Tao, W.Q., and Qiao, R., Predicting Effective Diffusivity of Porous Media from Images by Deep Learning, *Sci. Rep.*, vol. **9**, no. 1, pp. 1–12, 2019.

Wu, J., Yin, X., and Xiao, H., Seeing Permeability from Images: Fast Prediction with Convolutional Neural Networks, *Sci. Bull.*, vol. **63**, no. 18, pp. 1215–1222, 2018.

Xing, W., Elhabian, S.Y., Keshavarzzadeh, V., and Kirby, R.M., Shared-GP: Learning Interpretable Shared Hidden Structure Across Data Spaces for Design Space Analysis and Exploration, *J. Mech. Des.*, pp. 1–16, 2020.

Xing, W., Shah, A.A., and Nair, P.B., Reduced Dimensional Gaussian Process Emulators of Parametrized Partial Differential Equations Based on Isomap, *Proc. Roy. Soc. London a Math. Phys. Eng. Sci.*, vol. **471**, p. 2014–0697, 2015.

Xing, W., Triantafyllidis, V., Shah, A., Nair, P., and Zabaras, N., Manifold Learning for the Emulation of Spatial Fields from Computational Models, *J. Comput. Phys.*, vol. **326**, pp. 666–690, 2016.

Zhe, S., Xing, W., and Kirby, R.M., Scalable High-Order Gaussian Process Regression, *The 22nd International Conference on Artificial Intelligence and Statistics*, Naha, Okinawa, Japan, pp. 2611–2620, 2019.